

$^{29}\text{Si}\{^1\text{H}\}$ CP-MAS NMR comparison and ATR-FTIR spectroscopic analysis of the diatoms *Chaetoceros muelleri* and *Thalassiosira pseudonana* grown at different salinities

Sian M. La Vars · Martin R. Johnston · John Hayles ·
Jason R. Gascooke · Melissa H. Brown ·
Sophie C. Leterme · Amanda V. Ellis

Received: 16 October 2012 / Revised: 13 December 2012 / Accepted: 14 January 2013 / Published online: 31 January 2013
© Springer-Verlag Berlin Heidelberg 2013

Abstract Diatoms are key indicators of marine environmental health. To further understand how diatoms respond to varying degrees of salinity, either due to climate change or brine waste discharge into marine environments, two different diatom species were studied. *Thalassiosira pseudonana* and *Chaetoceros muelleri* were cultured at three different salinities namely, 26 practical salinity units (PSU or parts per thousand), 36 PSU (standard salinity for culturing of seawater species) and 46 PSU. Changes in silica and organic content within the cultured diatoms were analysed using solid-state $^{29}\text{Si}\{^1\text{H}\}$ cross-polarization–magic angle spinning (CP-MAS) nuclear magnetic resonance (NMR) and attenuated total reflection–Fourier transform infrared (ATR-FTIR) spectroscopies coupled with analysis of variance. ^{29}Si CP-MAS NMR showed that qualitatively the Q4:Q3 area ratios of *C. muelleri*, grown away from standard salinities, increased in response to the formation of more condensed ($2 \equiv \text{SiOH} \rightarrow \equiv \text{Si-O-Si} \equiv + \text{H}_2\text{O}$) and/or an increase in closely associated organic matter to the Q4 component of the diatoms. This was not observed for *T. pseudonana*. However, both species showed the appearance of a new peak centered at $1575\text{--}1580 \text{ cm}^{-1}$ in the ATR-FTIR spectra, designated as the C=N band of nitrogenous

purine-type compounds. Further, the *C. muelleri* species was shown to produce more extracellular polymeric substances at non-standard salinities. On this basis, results suggest that there is a strong relationship between diatom composition and salinity and that *C. muelleri* is more sensitive to its environment than *T. pseudonana*.

Keywords Diatoms · Salinity · ^{29}Si solid-state nuclear magnetic resonance · Fourier transform infrared spectroscopy

Introduction

Diatoms are unicellular eukaryotic organisms with an estimated 100,000 species found in salt and fresh water all around the world [1]. They contain nanopatterned cell walls built up of biomineralized silica (biosilica) [2]. This biomineralization process is believed to involve two important classes of biomolecules, namely highly phosphorylated silaffins [3] and long chain polyamines [4]. Current understanding is that the formation of the silicified cell wall is via intracellular transport of monosilicic acid [$\text{Si}(\text{OH})_4$] (present in natural environments at concentrations of 1–100 μM [5]) and subsequent polymerization occurs at a localized region within the diatom called a silicon deposition vesicle (SDV) [6, 7]. Within the SDV, lumen organic components such as polysaccharides and proteins have been suggested to influence silica morphogenesis, thus controlling biogenetic pathways in the formation of the characteristic diatom nanopatterns. This is believed to be achieved by influencing the kinetics of $\text{Si}(\text{OH})_4$ polycondensation and/or providing a template for silica nanoparticle deposition [8].

Previous studies have employed ^{29}Si , ^{13}C , ^1H , ^{15}N and ^{31}P solid-state nuclear magnetic resonance (NMR) spectroscopy in an attempt to understand the process of biomineralization.

S. M. La Vars · M. R. Johnston · J. R. Gascooke · A. V. Ellis (✉)
Flinders Centre for Nanoscale Science and Technology, School of
Chemical and Physical Sciences, Flinders University, Sturt Road,
Bedford Park, SA 5042, Australia
e-mail: amanda.ellis@flinders.edu.au

J. Hayles · M. H. Brown · S. C. Leterme
School of Biological Sciences, Flinders University, Sturt Road,
Bedford Park, SA 5042, Australia

S. C. Leterme
SARDI Aquatic Sciences, 2 Hamra Avenue,
West Beach, SA 5024, Australia

In particular, it has been successfully used to study the biochemical and elemental composition of various marine plankton [8, 9], the silicon uptake and metabolism of the diatom *Thalassiosira pseudonana* [2], as well as the characterization of diatom cell walls [10]. Similarly, liquid state ^{13}C and ^{29}Si NMR spectroscopy have been used for the analysis of lipids in *Neochloris oleoabundans* [11], compositional analysis of whole cells of *T. pseudonana* [12], compositional analysis of whole cells and lipid extracts of *C. muelleri* [13], analysis of humic substances and isolates of *Phaeodactylum tricoratum* [14], observation of the formation of hexavalent silicon complexes in *Navicula pelliculosa* [15] and the analysis of glucans extracted from diatoms [16, 17].

As a non-destructive technique, solid-state ^{29}Si NMR spectroscopy affords unique insights into the coordination of silicon atoms in biogenic silica within the diatom frustules. Of significance is that the technique can be used to observe alterations in the diatoms silica structure, such as the degree of hydroxylation ($-\text{OH}$ groups) or $-\text{O}-$ bridging (condensation).

Typical silicon environments observed in the ^{29}Si spectra of diatoms are designated [Q2] $\text{Si}(\text{OSi}\equiv)_2(\text{OH})_2$, [Q3] $\text{Si}(\text{OSi}\equiv)_3(\text{OH})$ and [Q4] $(\text{Si}(\text{OSi}\equiv))_4$, as shown in Fig. 1, where “n” of the Qn refers to the number of Si–O groups bonded to the central Si atom, with the structure becoming more rigid with the loss of the hydroxyl groups [2, 8, 10].

To date, solid-state ^{29}Si NMR spectroscopy has not been used to study the effects of changes in salinity on diatom molecular architectures. Salinity changes not only occur due to regular climate change and seasonal summer evaporation, but also as a result of the discharge of brine effluent into marine environments from industrial desalination plants. The effect of these salinity changes on the molecular architecture of diatoms may define the adaptability of certain diatom species.

In terms of understanding dynamic changes induced in diatom growth, Fourier transform infrared (FTIR) spectroscopy is another technique which provides invaluable, fast chemical characterization of, in particular, the organo-chemical components of diatoms. Investigations have used FTIR to study diatom interactions with heavy metal ions and acid–base equilibria [18], the effects of nitrogen deprivation [19],

understanding diatom valve formation and the organo-silica compounds involved in the process [20], elucidating chemical composition to determine nutritional status [21], and the formation of brucite $[\text{Mg}(\text{OH})_2]$ by the diatom *P. tricoratum* under stress [10]. FTIR spectroscopy has not previously been used to look at effects of changes in salinity on diatoms.

Here, we report on the structural and chemical characterization of the molecular architecture of biomineralized silica and organo-chemical functionalities of two centric diatom species, *C. muelleri* and *T. pseudonana* cultured at different salinities, namely 26, 36 and 46 PSU. Using solid-state ^{29}Si NMR and ATR-FTIR spectroscopies we show that *C. muelleri* appears to be more stressed by culturing in non-standard salinities and that they respond to changes in salinity by producing a more condensed silica structure and more proteinaceous materials.

Materials and methods

Diatom culturing

Cultures of *C. muelleri* (CS-176) and *T. pseudonana* (CS-20) diatom cells were obtained from the Australian National Algae Culture Collection (ANACC). Cells (25 mL) were inoculated into f/2 medium [22] (225 mL) at 26, 36 and 46 practical salinity units (PSU or parts per thousand). Salinities of ± 10 PSU from standard conditions for culture seawater algae (36 PSU) were chosen to reflect the increases and decreases of salinity in the environment, i.e. due to seasonal changes, drought, floods and/or brine discharge into marine environments. The cultures were grown with a light/dark photoperiod of 12 h/12 h at 20 °C for 14 days, after which the cultures were inoculated again in a 1:10 ratio (200 mL culture: 1,800 mL f/2 medium) to a total volume of 2 L, and grown under the same conditions for another 14 days to obtain the biomass required for the experiments. The sizes of the diatoms, using scanning electron microscopy (data not shown), were estimated to be 3 μm and 5.5 μm for *C. muelleri* and *T. pseudonana*, respectively.

$^{29}\text{Si}\{^1\text{H}\}$ CP-MAS NMR spectroscopy

In order to mitigate any potentially adverse changes in the polymerization state of the silica during harsh drying processes [8], such as freeze-drying, the diatom samples were dried by transferring either *C. muelleri* or *T. pseudonana* cells, in f/2 media, into Petri dishes and exposing them to a stream of nitrogen for 12 h. This process accelerates the drying process prior to the dried cells being placed in a desiccator ready for analysis. The samples were then measured by solid-state $^{29}\text{Si}\{^1\text{H}\}$ cross-polarization coupled to magic angle spinning (CP-MAS) spectroscopy at 22 °C on a

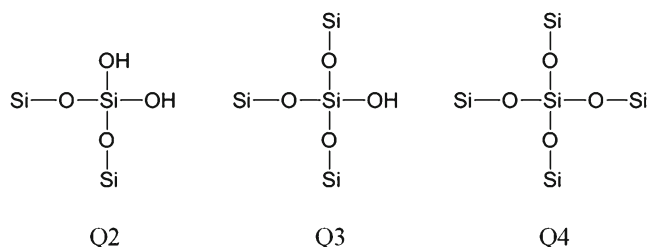


Fig. 1 Typical silicon environments observed in diatom frustules, Q2 (left), Q3 (centre) and Q4 (right)

Bruker 400 MHz Avance III UltraShield NMR spectrometer with Bruker MAS II with rotors (ZrO_2 ; diameter, 4 mm (Wilma Labglass)) containing ~100–200 mg of sample. The experimental details for the $^{29}Si\{^1H\}$ CP-MAS NMR experiments were as follows: ^{29}Si , 79.5 MHz; spinning rate 5 kHz; variable amplitude (ramp) contact time 2 ms; 90° 1H transmitter pulse length, 2.6 μs ; acquisition time 30 ms; repetition time, 3 s; number of scans 64–80,000. Peaks were referenced to sodium 2,2-dimethyl-2-silapentane-5-sulfonate at 0 ppm. Peak areas were determined by fitting the spectra to a sum of Gaussian functions using a non-linear least squares fitting algorithm. Errors in percentage peak areas and peak ratios were determined via a full propagation of errors analysis using the covariance matrix returned by the fitting algorithm [23].

ATR-FTIR spectroscopy

C. muelleri or *T. pseudonana* cells in f/2 media (1.25 mL) were pipetted into an Eppendorf tube and centrifuged (Eppendorf miniSpin Plus) for 30 min at 2,500 rpm (~2,300 $\times g$), after which the f/2 medium supernatant was discarded. Purified water (Millipore Milli-Q system) (1 mL) was then added and the samples were centrifuged for a further 20 min at 4,500 rpm (~4,100 $\times g$) and the supernatant discarded. This wash and centrifuge was repeated a further two times. The centrifugal forces (g -forces) used here have been previously shown to not damage the diatom cells [8]. The now washed diatom cells were then left to dry for 72 h in air. ATR-FTIR spectra were recorded on a PerkinElmer Spectrum 400 equipped with an ATR module.

The ATR crystal was zinc selenide with an angle of total reflection of 45° at 1000 cm^{-1} and a depth of radiation penetration (pathlength) of 6 μm . The ZnSe crystal had a refractive index of 2.4 and a 3 bounce system was used for measurements. The dried diatom samples were placed directly onto the ZnSe crystal and scans were performed with a resolution of 2.00 cm^{-1} over a range of $4000\text{--}650\text{ cm}^{-1}$,

with 16 scans per run. We estimate the penetration depth to be around 0.6–1.3 μm [24]. Each sample preparation was carried out in triplicate. All spectra were background subtracted and normalized to the Si–O–Si peak at 1062 cm^{-1} for *C. muelleri* and 1063 cm^{-1} for *T. pseudonana*.

Statistical analyses of ATR-FTIR spectra

Different regions of the ATR-FTIR spectra corresponding to the functional group/structure are presented in Table 1. Data of peak intensities for each functional group/structure were not normally distributed (Kolmogorov–Smirnov test, $p < 0.001$) and were square-root transformed before being normalized. An Euclidian resemblance matrix was subsequently created using PRIMER-E v.6 and a two-way mixed model PERMANOVA (maximum permutations=9,999) was used to test differences between species (i.e. *C. muelleri* and *T. pseudonana*) and salinity treatments (26, 36 and 46 PSU), which were used as factors. When the main PERMANOVA tests were significant pairwise tests were conducted to determine which factors were responsible for significance.

Results and discussion

$^{29}Si\{^1H\}$ CP-MAS NMR study of *C. muelleri* and *T. pseudonana* cells

The CP NMR technique is based on the signal enhancement of a low abundance or low magnetogyric ratio (γ) nucleus X via the transfer of polarization from a high-abundance and high magnetogyric ratio nucleus (such as 1H) and can be used here to study ^{29}Si [29]. The efficiency of the X{ 1H } CP transfer to ^{29}Si depends on the distance between the two nuclei. However, this distance-dependence of the signal intensity also implies that the resulting data are only qualitative. Nonetheless, this technique provides valuable information for comparing the spectra of the diatoms grown at various salinities.

Table 1 Typical functional group and structure assignment for peaks observed in FTIR spectra of diatoms

Wavenumber (cm^{-1})	Functional group/structure ^a	Reference
3280	$\nu(O-H)$, $\nu(N-H)$, water, carboxylic acids	[18, 20, 25]
3010, 2950, 2920, 2850	$\nu(C-H)$, $\nu(CH_2)$, $\nu(CH_3)$, lipids	[18, 19, 24, 26]
1730–1740	Ester groups, fatty acids and lipids	[18–20, 26]
1650–1630	$\nu(C=O)$ (Amide I), proteins, silica	[19, 20, 25–27]
1540, 1570	N–H bending (Amide II), proteins	[18–20, 26, 27]
1430, 1460	CH_2 , CH_3 , C–O, COO^- , proteins	[19, 20, 26]
1410–1420	Carboxylic acids	[18]
1380	CH_2 , CH_3 , C–O, COO^- bending, proteins	[19, 26]
1060	sym $\nu(Si-O-Si)$, polysaccharides	[18–20, 26, 28]
700–800	sym $\nu(O-Si-O)$, sym $\nu(Si-O-Si)$	[18, 20, 28]

^a ν is a stretch, *sym* is symmetrical vibration

The $^{29}\text{Si}\{^1\text{H}\}$ CP-MAS NMR spectra of *C. muelleri* and *T. pseudonana* cells grown in salinities 26, 36 and 46 PSU are shown in Fig. 2a and b, respectively.

Visible in the spectra are the typical patterns of amorphous silica with resolved Q2 ($\delta=-93$ ppm), Q3 ($\delta=-102$ ppm), and Q4 ($\delta=-112$ ppm) signals [29]. No peaks were observed that could be attributed to monosilicic acid (approximately -70 ppm), or to higher coordinated silica structures of hyper-coordinated organo-silicon complexes (approximately -120 ppm) [8]. In particular, monosilicic acid has been suggested as being a silica precursor compound [8].

The broad line widths reflect disordered local ^{29}Si environments due to a large distribution of compounds, bond lengths and/or bond angles [30]. Interestingly, for *C. muelleri* cultured at 36 PSU (Fig. 2(a)) the line width of the Q2-based silicon peak (centred at -93.0 ± 0.1 ppm) is narrower and the peak itself more pronounced than at other salinities.

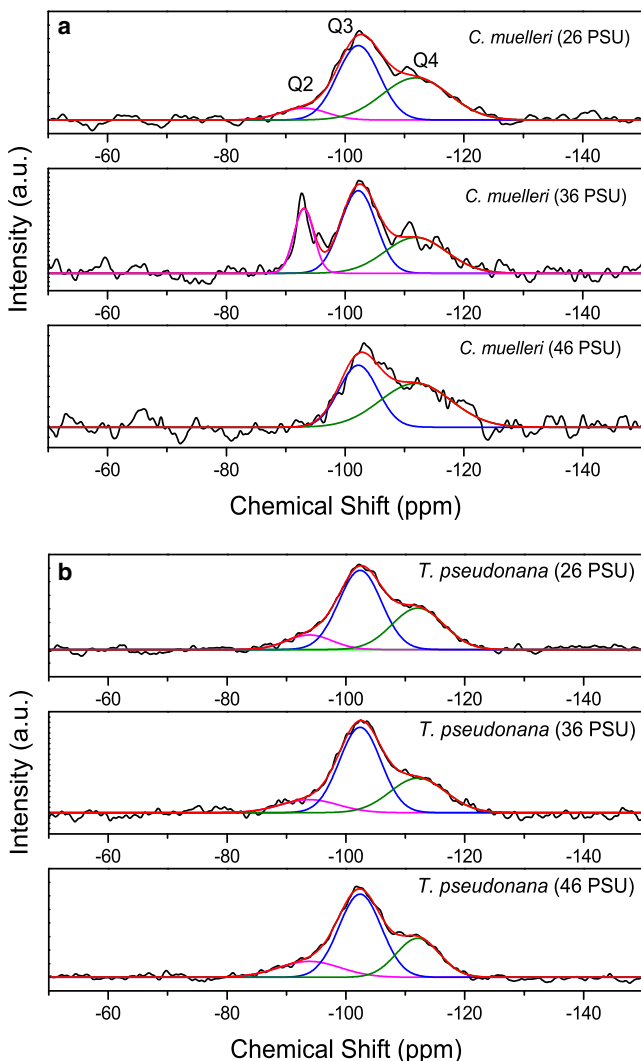


Fig. 2 Qualitative comparison of overlaid solid-state $^{29}\text{Si}\{^1\text{H}\}$ CP-MAS NMR spectra of **a** dried *C. muelleri* and **b** dried *T. pseudonana* whole cells grown in 26, 36 and 46 PSU

This may indicate a more specific type of compound associated with this species.

In the interests of preparing comparative data, Gaussian fits were performed on the spectra. During the fitting procedure, it was found that the Q n peak positions remained constant (within fitting error) for diatoms cultured in various salinities. For reliable determinations of the peak areas, all spectra were fitted simultaneously with common peak positions, whilst the peak width and peak area were allowed to vary for each peak in the spectrum. The peak maxima, percentage peak areas and Q4:Q3 ratios are shown in Table 2.

For *C. muelleri*, it is clear that when cultured under standard salinity for seawater species (36 PSU) there was a greater contribution (20.1 ± 0.7) from Q2-based silicon (at -93.0 ± 0.1 ppm) compared to diatoms cultured at 26 PSU (8.5 ± 1.6) and 46 PSU (not detectable); see Table 2. Interestingly, the Q3-based silicon [$\text{Si}(\text{OSi}\equiv)_3(\text{OH})$] content at -102.2 ± 0.2 ppm remained mostly unchanged at 48.2 ± 4.7 , 45.7 ± 4.3 and 43.5 ± 3.8 for 26, 36 and 46 PSU, respectively. The more condensed Q4-based silicon content [$\text{Si}(\text{OSi}\equiv)_4$], observed at -111.8 ± 0.6 ppm, increased as *C. muelleri* was cultured in salinities away from 36 PSU (34.3 ± 4.2) to 43.4 ± 4.3 at 26 PSU and 56.5 ± 3.8 at 46 PSU. This lower Q2 content and higher Q4 content of the *C. muelleri* cultured away from 36 PSU indicates that these diatoms have a more condensed silicon structure and/or organic material that is tightly bound to the silica. With potentially lower hydroxyl group content, and thus more hydrophobic and rigid frustules the passage of nutrients into the silica network may be inhibited [31]. In this case, it may be that when *C. muelleri* diatoms are stressed by culturing in non-standard salinities that they change their silica structure in the frustules in order to regulate osmosis [31].

For comparative analysis, it is appropriate to compare Q4/Q3 area ratios between the different salinities for a given species rather than between species at a given salinity. These Q4/Q3 area ratios (Table 2) were then used to try and identify which salinity had the more profound effect on the diatom cells. Table 2 shows that

Table 2 Deconvoluted peak chemical shifts (ppm) and associated calculated percentage areas for *C. muelleri*. Quoted errors are 2 standard deviations (95 % confidence interval)

	CM 26 PSU % area	CM 36 PSU % area	CM 46 PSU % area
Q2 (-93.0 ± 0.1 ppm)	8.5 ± 1.6	20.1 ± 0.7	–
Q3 (-102.2 ± 0.2 ppm)	48.2 ± 4.7	45.7 ± 4.3	43.5 ± 3.8
Q4 (-111.8 ± 0.6 ppm)	43.4 ± 4.3	34.3 ± 4.2	56.5 ± 3.8
Q4:Q3 Area ratio	0.90 ± 0.18	0.75 ± 0.16	1.30 ± 0.20

for *C. muelleri* the Q4/Q3 area ratios appear highest at 46 PSU (1.30 ± 0.20), followed by 26 PSU (0.90 ± 0.18), and finally the lowest at 36 PSU (0.75 ± 0.16). This change or increase in Q4/Q3 area ratio away from standard salinities may be a result of increased silicon condensation and/or increase in organic material in intimate contact with the Q4-type silica. This implies that there may be a change in biosilification as *C. muelleri* attempts to adapt to changes in salinities. Further, higher salinities may require a stronger need to regulate osmotic flow into the cells than lower salinities.

On the contrary when *T. pseudonana* was cultured at different salinities there were no dramatic changes in the Q2-, Q3- or Q4-based silicon content (see Table 3). This would indicate that *T. pseudonana*, unlike *C. muelleri*, is reasonably unaffected by changes in salinity.

FTIR-ATR study of *C. muelleri* and *T. pseudonana* cells

Figure 3A and B show the overlaid normalized FTIR-ATR spectra of dried washed (A) *C. muelleri* and (B) *T. pseudonana* whole cells cultured in salinities of (a) 26 PSU, (b) 36 PSU and (c) 46 PSU, respectively. Typical peak assignments are shown in Table 1. Vibrations attributed to the aliphatic region between 3010–2850 cm^{-1} and the silica network between 1250–900 cm^{-1} of both species do not appear to alter greatly between salinities (Fig. 3A and B). However, for each species there does appear to be stronger absorption features in the amide II region [18–20, 26, 27] at 1500–1590 cm^{-1} (region marked between dotted lines) for the diatoms cultured at 26 and 46 PSU (Fig. 3A(a) and B(c), respectively) than at 36 PSU (Fig. 3A(b)). In Fig. 3A and B, for both 26 PSU (a) and 46 PSU (c), the overall intensities of the amide II peaks (region marked between dotted lines) for the different species relative to the amide I bands between 1628–1631 cm^{-1} is far higher than at 36 PSU (b). This is in good agreement with findings by Fujui et al. [32] who used gas chromatography–mass spectrometry to show that *C. muelleri* grown at elevated salinities (>50 mM NaCl)

Table 3 Deconvoluted peak chemical shifts (ppm) and associated calculated percentage areas for *T. pseudonana*. Quoted errors are 2 standard deviations (95 % confidence interval)

	TP 26 PSU % area	TP 36 PSU % area	TP 46 PSU % area
Q2 (−93.9±0.6 ppm)	10.7±1.6	12.0±1.5	15.9±2.0
Q3 (−102.4±0.1 ppm)	54.6±2.7	57.1±2.2	56.9±2.7
Q4 (−112.1±0.2 ppm)	34.7±1.4	30.9±1.1	27.2±1.1
Q4/Q3 Area ratio	0.64±0.06	0.54±0.04	0.48±0.04

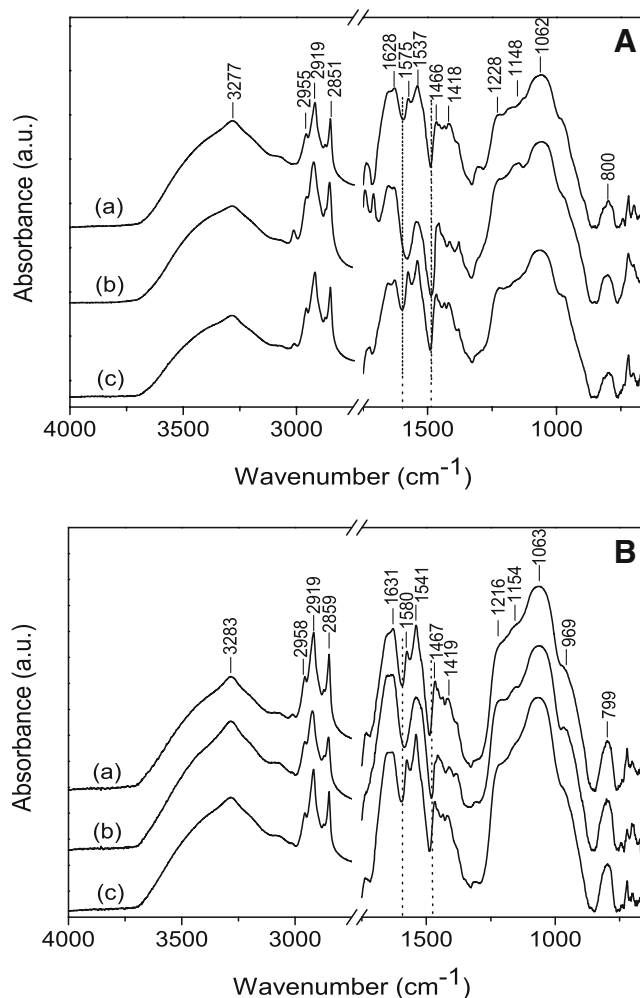


Fig. 3 Normalized FTIR-ATR spectra of dried washed **A** *C. muelleri* and **B** *T. pseudonana* cells grown in different salinities (a) 26 PSU, (b) 36 PSU and (c) 46 PSU. The spectra have been offset for convenience of viewing

exhibited a gradual increase in the free amino acid, glutamic acid. They proposed that this increase in amino acid production acted as a strong contributor to osmoregulation in the species. Here, we observed an increased protein production, perhaps in response to osmoregulation of these species at salinities away from 36 PSU. An important consideration then is how this may contribute to an increase in extracellular polymeric substance (EPS) production in harsh environments. Furthermore, the amide II bands in both (a) and (c) spectra are split into two with the evolution of an interesting unusual weaker but well-resolved peak at ~1575–1585 cm^{-1} in both species grown away from standard salinities. Moreover, the band centred at ~1650 cm^{-1} may also be a combination of several groups (other than amide I). Its nonsymmetrical shape and the broadness show the complexity of its composition. Absorptions due to C=C and C=N stretching vibrations are expected in this region of frequencies. Tsuboi et al. [33]

Table 4 Summary of the PER-MANOVA tests

FTIR range (cm ⁻¹)	Significant difference between species	Significant difference for <i>T. pseudonana</i>	Significant difference for <i>C. muelleri</i>
Entire spectra	$P < 0.05$		36,46 PSU; $P < 0.05$
3100–3800			
1800–3100			36,46 PSU; $P < 0.05$ 36,26 PSU; $P < 0.05$
1680–1800	$P < 0.05$		36,46 PSU; $P < 0.05$ 36,26 PSU; $P < 0.05$
1590–1680	$P < 0.05$		36,46 PSU; $P < 0.05$ 36,26 PSU; $P < 0.05$
1560–1590		36,46 PSU; $P < 0.05$ 36,26 PSU; $P < 0.05$	36,46 PSU; $P < 0.05$ 36,26 PSU; $P < 0.05$
1500–1560			36,46 PSU; $P < 0.05$ 36,26 PSU; $P < 0.05$
1400–1500	$P < 0.05$		36,46 PSU; $P < 0.05$ 36,26 PSU; $P < 0.05$
900–1300	$P < 0.05$		36,46 PSU; $P < 0.05$ 36,26 PSU; $P < 0.05$

assigned calculated frequencies at 1631 and 1582 cm⁻¹ to $\nu(\text{C}=\text{C})$ and $\nu(\text{C}=\text{N})$, respectively, with a contribution to each of these frequencies of $\nu(\text{C}-5-\text{C}-6)$. In particular, the C=N band at 1575 cm⁻¹ has previously been assigned to adenine [34, 35].

Further compositional changes can be observed in the region of the ester carbonyl stretching vibrations (at approximately 1750 cm⁻¹) in particular Fig. 3A(b) for *C. muelleri* at 36 PSU, but not for *T. pseudonana* (Fig. 3A(b)). Two bands are present which are more intense relative to the neighbouring bands, i.e. to the protein-related amide I/II bands at ~1628–1500 cm⁻¹, than at both 46 PSU (a) and 26 PSU (c). This may correlate with a possible higher content of lipids, as the corresponding fatty-acid C–H stretching region (~2840–3000 cm⁻¹) in spectrum (b) appears relatively more intense.

PERMANOVA tests of the FTIR-ATR spectra indicated that *C. muelleri* cultured at non-standard salinities (26 and 46 PSU) showed significant differences in some of the functional groups/structure identified in Table 1. The significant changes were mainly in functional groups/structure corresponding to amino acids and proteins in the region 1560–1590 cm⁻¹ (Table 4). Hecky et al. [36] suggested that proteins with hydroxyl-containing amino acids may be involved in templating the diatom silica structure by forming ester bonds through a condensation reaction with silicic acid. In particular, the structural availability of the amino acids as nucleation sites could determine the degree of cross-linking between the silica and the protein template. This would then suggest that salinity has an impact on the templating of the diatom silica. This would suggest that *C. muelleri* produced higher amounts of EPS at salinities away from 36 PSU, which may be indicative of the diatom experiencing stress [37] and as such produce more mucilage than the diatoms in 36 PSU (Table 4). It has indeed been shown in previous studies that EPS is linked to extracellular mechanisms of diatom cell protection at high salinities [38]. Interestingly, there is a significance difference away from

standard salinities for both species in the 1560–1590 cm⁻¹ region of the spectra. Thus, both species produce this particular C=N nitrogenous purine-based material when stressed.

Conclusion

In summary, we present results of solid-state ²⁹Si{¹H} CP-MAS NMR spectra without any extraction or silica dissolution of diatoms thus preserving frustule integrity. The study sheds new light on the differences in two different diatom species *C. muelleri* and *T. pseudonana* abilities to adapt to various changes in salinity. *C. muelleri* diatom cells have been shown to be the most affected by salinity with changes by up to ±10 PSU. However, they are more greatly affected by high salinities (46 PSU) rather than lower ones (26 PSU) in which they produce more condensed, hydrophobic and rigid silica structures and/or organic material closely linked to the condensed silica. They also appear to respond to salinity changes by producing more proteinaceous materials which may impact on the templating of the diatom silica. In both species, a new peak appeared between 1560 and 1590 cm⁻¹ in the ATR-FTIR spectra as the diatoms were cultured away from standard conditions this peak has been assigned to nitrogenous purine-type compounds. Finally, *C. muelleri* was also been shown to produce more EPS compared to *T. pseudonana* which may help combat the changes in salinity for this species.

This study is an important step towards the advancement in monitoring the potential adaptation strategies of diatoms with changes in salinity, either due to discharge of brine effluent from desalination plants or climate change.

Acknowledgments The authors wish to acknowledge the financial support of an ARC Discovery Grant (DP110101679) and the National Centre of Excellence in Desalination Australia which is funded by the Australian Government through the Water for the Future initiative. We thank the Australian Research Council for a LIEF grant (LE0668489) for the purchase of the NMR spectrometer. We also thank Matthieu Bourgeois for his assistance with the algal culture.

References

- Falciatore A, Bowler C (2002) Revealing the molecular secrets of marine diatoms. *Annu Rev Plant Biol* 53(1):109–130
- Gröger C, Sumper M, Brunner E (2008) Silicon uptake and metabolism of the marine diatom *Thalassiosira pseudonana*: solid-state ²⁹Si NMR and fluorescence microscopic studies. *J Struct Biol* 161(1):55–63
- Kröger N, Lorenz S, Brunner E, Sumper M (2002) Self-assembly of highly phosphorylated silaffins and their function in biosilica morphogenesis. *Science* 298:584–586
- Sumper M (2002) A phase separation model for the nanopatterning of diatom biosilica. *Science* 295:2430–2433
- Del Amo Y, Brzezinski MA (1999) The chemical form of dissolved Si taken up by diatoms. *J Phycol* 35:1162–1170
- Vrieling EG, Beelen TPM, van Santen RA, Gieskes WWC (1999) Silicon deposition in diatoms: control by the pH inside the silicon deposition vesicle. *J Biotechnol* 70:39–51
- Kröger N, Poulsen N (2008) Diatoms—from cell wall biogenesis to nanotechnology. *Annu Rev Genet* 42:83–107
- Brunner E, Gröger C, Lutz K, Richthammer P, Spinde K, Sumper M (2009) Analytical studies of silica biomineralization: towards an understanding of silica processing by diatoms. *Appl Microbiol Biotechnol* 84(4):607–616
- Hedges JI, Baldock JA, Gélinais Y, Lee C, Peterson ML, Wakeham SG (2002) The biochemical and elemental compositions of marine plankton: a NMR perspective. *Mar Chem* 78(1):47–63
- Tesson B, Gaillard C, Martin-Jézéquel V (2008) Brucite formation mediated by the diatom *Phaeodactylum tricornutum*. *Mar Chem* 109(1–2):60–76
- Beal CM, Webber ME, Ruoff RS, Hebner RE (2010) Lipid analysis of *Neochloris oleoabundans* by liquid state NMR. *Biotechnol Bioeng* 106(4):573–583
- Chauton MS, Størseth TR, Johnsen G (2003) High-resolution magic angle spinning ¹H NMR analysis of whole cells of *Thalassiosira pseudonana* (Bacillariophyceae): broad range analysis of metabolic composition and nutritional value. *J Appl Phycol* 15(6):533–542
- Chauton MS, Størseth TR, Krane J (2004) HR MAS DEPT 13C NMR analysis of whole cells of *Chaetoceros muelleri* (Bacillariophyceae), and comparison with 13C NMR and DEPT 13C NMR analysis of lipophilic extracts. *J Phycol* 40(3):611–618
- Gillam AH, Wilson MA (1985) Pyrolysis-GC–MS and NMR studies of dissolved seawater humic substances and isolates of a marine diatom. *Org Geochem* 8(1):15–25
- Kinrade SD, Gillson A-ME, Knight CTG (2002) Silicon-29 NMR evidence of a transient hexavalent silicon complex in the diatom *Navicula pelliculosa*. *J Chem Soc Dalton Trans*, 307–309
- Størseth TR, Hansen K, Skjermo J, Krane J (2004) Characterization of a β-D-(1→3)-glucan from the marine diatom *Chaetoceros muelleri* by high-resolution magic-angle spinning NMR spectroscopy on whole algal cells. *Carbohydrate Res* 339(2):421–424
- Størseth TR, Kirkvold S, Skjermo J, Reitan KI (2006) A branched β-D-(1→3,1→6)-glucan from the marine diatom *Chaetoceros debilis* (Bacillariophyceae) characterized by NMR. *Carbohydrate Res* 341(12):2108–2114
- Gélalbert A, Pokrovsky OS, Schott J, Boudou A, Feurtet-Mazel A, Mielczarski J, Mielczarski E, Mesmer-Dudons N, Spalla O (2004) Study of diatoms/aqueous solution interface. I. Acid–base equilibria and spectroscopic observation of freshwater and marine species. *Geochim Cosmochim Acta* 68(20):4039–4058
- Giordano M, Kansiz M, Heraud P, Beardall J, Wood B, McNaughton D (2001) Fourier Transform Infrared spectroscopy as a novel tool to investigate changes in intracellular macromolecular pools in the marine microalga *Chaetoceros muellerii* (bacillariophyceae). *J Phycol* 37(2):271–279
- Heredia A, van der Strate HJ, Delgadillo I, Basiuk VA, Vrieling EG (2008) Analysis of organo–silica interactions during valve formation in synchronously growing cells of the diatom *Navicula pelliculosa*. *Chem BioChem* 9(4):573–584
- Hirschmugl CJ, Bayarri Z-E, Bunta M, Holt JB, Giordano M (2006) Analysis of the nutritional status of algae by Fourier transform infrared chemical imaging. *Infrared Phys Tech* 49(1–2):57–63
- Guillard RRL, Ryther JH (1962) Studies of marine planktonic diatoms. I. *Cyclotella nana* Hustedt and *Detonula confervacea* (Cleve). *Gran Can J Microbiol* 8:229–239
- Bevington PR, Robinson KD (2003) Data reduction and error analysis for the physical sciences, 3rd edn. McGraw-Hill, USA
- Gélalbert A, Pokrovsky OS, Schott J, Boudou A, Feurtet-Mazel A, Mielczarski J, Mielczarski E, Mesmer-Dudons N, Spalla O (2004) Study of diatoms/aqueous solution interface. I. Acid–base equilibria and spectroscopic observation of freshwater and marine species. *Geochim Cosmochim Acta* 68(20):4039–4058
- Kammer M, Hedrich R, Ehrlich H, Popp J, Brunner E, Krafft C (2010) Spatially resolved determination of the structure and composition of diatom cell walls by Raman and FTIR imaging. *Anal Bioanal Chem* 398(1):509–517
- Stehfest K, Toepel J, Wilhelm C (2005) The application of Microscopy FTIR spectroscopy to analyse nutrient-stress related changes in biomass composition of phytoplankton algae. *Plant Physiol Biochem* 43(7):717–726
- Jiang W, Saxena A, Song B, Ward BB, Beveridge TJ, Myneni SCB (2004) Elucidation of functional groups on gram-positive and gram-negative bacterial surfaces using infrared spectroscopy. *Langmuir* 20(26):11433–11442
- Yuan P, Wu DQ, He HP, Lin ZY (2004) The hydroxyl species and acid sites on diatomite surface: a combined IR and Raman study. *Appl Surf Sci* 227(1–4):30–39
- Tesson B, Masse S, Laurent G, Maquet J, Livage J, Martin-Jézéquel V, Coradin T (2008) Contribution of multi-nuclear solid state NMR to the characterization of the *Thalassiosira pseudonana* diatom cell wall. *Anal Bioanal Chem* 390:1889–1898
- Christiansen SC, Hedin N, Epping JD, Janicke MT, del Amo Y, Demarest M, Brzezinski MA, Chmelka BF (2006) Sensitivity considerations in polarization transfer and filtering using dipole–dipole couplings: implications for biomineral systems. *Solid State Nucl Mag* 29:170–182
- Vrieling EG, Sun Q, Tlan M, Kooyman PJ, Gieskes WWC, van Santen RA, Sommerdijk NAJM (2007) Salinity-dependent diatom biosilicification implies an important role of external ionic strength. *Proc Nat Acad Sci USA* 104(25):10441–10446
- Fujii S, Nishimoto N, Notoya A, Hellebust JA (1995) Growth and osmoregulation of *Chaetoceros muelleri* in Relation to Salinity. *Plant Cell Physiol* 36(5):759–764
- Tsuboi M, Takahashi S, Harada I (1973) In: Duchesne J (ed) Infrared and Raman spectra of nucleic acids–vibrations in the base residues. In physico-chemical properties of nucleic acids, 2nd edn. Academic, New York, pp 91–145
- Movasaghi Z, Rehman S, Rehman IU (2008) Fourier transform infrared (FTIR) spectroscopy of biological tissues. *Appl Spectrosc Rev* 43:134–179
- Dovbeshkoa GI, Gridinab NY, Kruglovac EB, Pashchuka OP (2000) FTIR spectroscopy studies of nucleic acid damage. *Talanta* 53(1):233–246
- Hecky RE, Mopper K, Kilham P, Degens ET (1973) The amino acid and sugar composition of diatom cell walls. *Mar Biol* 19:323–331
- Smith DJ, Underwood GJ (1998) Exopolymer production by intertidal epipellic diatoms. *Limnol Oceanogr* 43(7):1578–1591
- Krembs C, Eicken H, Junge K, Deming JW (2002) High concentrations of exopolymeric substances in Arctic winter sea ice: implications for the polar ocean carbon cycle and cryoprotection of diatoms. *Deep-Sea Res* 1 Oceanogr Res Pap 49:2163–2218